Journal of
Ceramic Science
and Technology

J. Ceram. Sci. Tech., **03** [04] 189-198 (2012)
DOI: 10.4416/JCST2012_00021
available online at: http://www.ceramic-science.com

Ytterbia-Neodymia Costabilized Zirconia – Alumina Nanocomposites

F. Kern*

Universität Stuttgart, Institut für Fertigungstechnologie keramischer Bauteile
University of Stuttgart, Institute for Manufacturing Technologies of
Ceramic Components and Composites, D-70569 Stuttgart, Allmandring 7B
received June 12, 2012; received in revised form September 19, 2012; accepted October 2, 2012

Abstract

Alumina-toughened zirconia composites are attractive materials for biomedical and demanding mechanical engineering applications as the added alumina increases hardness and strength while the fracture toughness of zirconia is preserved. In the present study an unstabilized pyrogenic zirconia nanopowder was coated with 1 mol% ytterbia and 2 mol% neodymia via the nitrate route, the powder was blended with 20 vol% submicron size alumina. Samples were hot-pressed at 1250 – 1450 °C for 1 h at 60 MPa axial pressure. Microstructure, phase composition and mechanical properties were investigated. The composites show proceeding phase separation with rising sintering temperature. Cubic precipitates are formed, leaving a highly transformable tetragonal zirconia matrix, which results in a combination of very high fracture resistance, threshold stress intensity and bending strength. The material thus combines high resistance to catastrophic failure in single loading events and good prospects for applications operating under cyclical loading conditions.

Keywords: Ceramics, mechanical properties, phase composition, microstructure

I. Introduction

The high strength and toughness of zirconia ceramics result from the stress-induced martensitic transformation of metastable tetragonal phase to stable monoclinic phase. This transformation is associated with volume expansion (~ 5 %) and shear. In the wake of the crack a process zone is formed which shields the crack and slows or stops crack propagation. The metastability of the tetragonal phase is achieved by stabilization of zirconia with metal oxides such as magnesia or yttria [1].

Zirconia ceramics may be divided in two main groups, partially stabilized zirconia (PSZ) like Mg-PSZ and Ca-PSZ in which lenticular tetragonal zirconia precipitates are incorporated into a coarse cubic matrix. Tetragonal zirconia polycrystals (TZP) are fine-grained and the tetragonal phase makes up the majority of the material [2]. Today engineering ceramics for biomedical applications are TZP or TZP-alumina composites [3]. The standard TZP material is yttria-stabilized zirconia (Y-TZP), which is commonly stabilized with 2.5 – 3.5 mol% yttria. Y-TZP has high strength (800 – 1500 MPa) but only exhibits moderate toughness (4 – 6 MPa·√m). The inverse strength-toughness relation is achieved by stabilization with tetravalent ceria. Here the toughness is high (> 10 MPa·√m), but strength limited (300 – 500 MPa) [4]. The characteristics of various other trivalent, tetravalent and charge-compensating stabilizer oxides have been studied in detail, but most systems have no technical relevance for structural ceramics [5 – 7].For fuel cells and thermal barrier coatings, rare-earth-oxide-doped zirconia, but with higher stabilizer concentrations, has high relevance [8, 9]. The state-the-art method of stabilizing, leading to homogeneous stabilizer distribution, is coprecipitation of stabilizer and zirconia from salt solutions [10]. Various authors have reported on the coating of monoclinic powder with stabilizer or high-energy co-milling [11 – 13]. Y-TZP materials manufactured from coated powders show improved toughness and aging resistance [14, 15]. The addition of small amounts of alumina to zirconia leads to incorporation of the alumina into the grain boundaries as shown by Ross [16]. This improves the low-temperature aging resistance and changes the strength toughness and grain growth characteristics [17]. Higher amounts of added alumina lead to alumina-toughened zirconia (ATZ), a material that shows drastically improved aging resistance, improved strength and hardness at similar toughness [18, 19]. Swain has shown that ATZ has smaller defect sizes than TZP [4].

Costabilization of TZP with different tri- and tetravalent dopants have been shown, e.g. by Kan and Huang [20 – 22]. High toughness has been found in yttria-neodymia-stabilized TZP [23]. YNd-TZP has been successfully applied as a matrix in electrically conductive composites [24 – 25]. It has been claimed that yttria-neodymia-costabilized zirconia has higher hydrothermal stability than Y-TZP [26]. Gadow and Kern have shown that 1.5Y-1.5Nd-TZP-alumina composites have higher strength than 1.5Y-1.5Nd-TZP but retain its high toughness [27]. The high strength and toughness in 1Y-2Nd-TZP derived from coated nanopowders was correlated to a phase separation process affecting the microstructure, which segregates in-

* Corresponding author: frank.kern@ifkb.uni-stuttgart.de

to extremely fine grain transformable tetragonal matrix and untransformable cubic precipitates [28]. Ytterbia-stabilized zirconia Yb-TZP shows high toughness and higher strength than Y-TZP [29,30].

In this study ytterbia-neodymia codoping was tried in combination with alumina addition to produce 1Yb-2Nd-ATZ with the aim of investigating microstructure, phase composition and strength-toughness correlations in comparison to the recently investigated 1Y-2Nd-TZP- and 1Gd-2Nd-TZP-based systems [28,31]. A nanoscale starting powder in combination with hot pressing was chosen in order to obtain full density at low sintering temperature and to test the evolution of properties over a wide range of sintering temperatures.

The motivation to obtain higher toughness, even if this does not lead to higher strength, is not as evident as for an intrinsically flawless and perfectly machined 3Y-TZP, implemented under controlled loading conditions. In such a case toughness is not so relevant for component performance. If, however, the part is manufactured with technologies such as injection moulding which systematically produce larger microstructural defects than e.g. cold isostatic pressing, higher toughness is definitely beneficial. The same is true in applications where the components are susceptible to damage by machining (e.g. manual dressing of dental implants, crowns or bridges) or operation (scratching, multiaxial loading) and in the case of component design that is not specifically adapted to ceramics, which sometimes cannot be avoided.

II. Experimental

The starting powders for this study were unstabilized zirconia VP-Ph (Evonik, Germany, $S_{BET} = 60\ m^2/g$) and α-alumina APA0.5 (Ceralox, USA, $S_{BET} = 8\ m^2/g$). The zirconia was coated via the nitrate route with 1 mol% Yb_2O_3 and 2 mol% Nd_2O_3 neodymia (both Chempur, Germany, 99.9 % purity) basically following the procedure devised by Yuan [13]. A coating procedure adapted to ultrafine zirconia was previously described in detail by the author [29]. The resulting calcined powder was blended with 20 vol% alumina and milled for 4 h in 2-propanol using Y-TZP balls (d = 1 mm). After separation of the milling media, the ATZ blend was dried and screened. Samples were consolidated by means of hot pressing (KCE, Germany) at 1250 °C – 1450 °C for 1 h under 60 MPa axial pressure. The resulting plates with dimensions of 42 x 22 x 2 mm³ were lapped with 15 μm diamond suspension, polished with 15 – 1 μm diamond suspension and cut into bending bars. Sides and edges of the bars were carefully ground and polished to eliminate machining defects. The final dimensions of the bars were 3.8 (±0.1) x 1.7 (±0.1) x 22 mm³. The microstructure of polished and thermally etched surfaces (1200 °C/10 min/air) with a conductive PdPt coating was investigated by means of SEM (Zeiss, Germany) in SE mode at 3 kV acceleration voltage. EDX measurements were performed on the same SEM. The phase composition was measured on polished surfaces and fracture faces by integrating the areas of monoclinic and tetragonal XRD reflexes in the 27 – 33° 2θ-range applying the calibration curve of Toraya (Bruker D8, Germany, CuKα, graphite monochromator) [32]. Measurement of the mechanical properties included measurement of Vickers hardness HV_{10} (Bareiss, Germany, five indents) and $HV_{0.1}$ (Fischer, Germany, 12 indents), determination of the indentation modulus E_{IND} and the measurement of 4-pt bending strength in a setup with 10 mm inner and 20 mm outer span at a crosshead speed of 2.5 mm/min (ten samples). The indentation modulus was determined according to the universal hardness method from the loading/unloading curve of the $HV_{0.1}$ microhardness measurement. Fracture resistance was determined with three methods in order to be able to compare with existing literature data. Indentation fracture resistance K_{IND} was determined by means of direct crack length measurement according to Anstis on five HV_{10} indents [33]. Fracture resistance by indentation strength in bending K_{ISB} was measured according to Chantikul based on determination of the residual strength (in the same 4-pt setup) of four bars pre-indented with a HV_{10} indent in the middle of the tensile side [34]. In order to determine the threshold stress intensity, stable indentation crack growth in flexure was measured in the same 4-pt setup at a crosshead speed of 5 mm/min. The procedure was proposed by Braun and refined by Dransmann [35,36]. The experimental procedure closely followed the protocol described by Benzaid [37]. Samples were pre-indented with four HV_{10} indents each with the diagonals parallel and perpendicular to the sides at 2 mm distance in the middle of the tensile side of a bending bar. The samples were then stored for two weeks to allow the cracks to grow subcritically to a stable extension. Samples were initially loaded with 30 % of their residual strength (determined in ISB test). The load was subsequently increased in 50 – 100-MPa increments until fracture. The length of the cracks perpendicular to the sides was measured after each loading step. A plot of the applied stress intensity $K_{appl} = \psi \cdot \sigma \cdot \sqrt{c}$ versus the residual indentation stress intensity $K_{res} = P \cdot c^{-1.5}$ allows the determination of the subcritical stress intensity K_0. If $K_{res} > K_{appl}$, no crack growth occurs. The onset of crack growth, visible from the kink in the curve, is the value $K_{appl,0}$. The fracture toughness is obtained at the intercept of the straight linear part with the slope χ starting from the kink and the ordinate. The threshold K_0 is given by $K_0 = K_{Ic} - K_{appl,0}$ [37]. The parameters for the calculation are the indentation load P = 98.1 N, the crack geometry parameter $\psi = 1.27$, the measured crack length c in μm, and the stress σ in MPa. Lube and Fett have shown that in the case of material with R-curve behaviour the extrapolation to the ordinate intercept can lead to unrealistically high values for the fracture resistance [38]. Moreover in the case of R-curve behaviour, the fracture resistance rises with crack length, thus K_{Ic} has no fixed value. It was therefore assumed that K_{ISB} is the upper boundary of the fracture resistance.

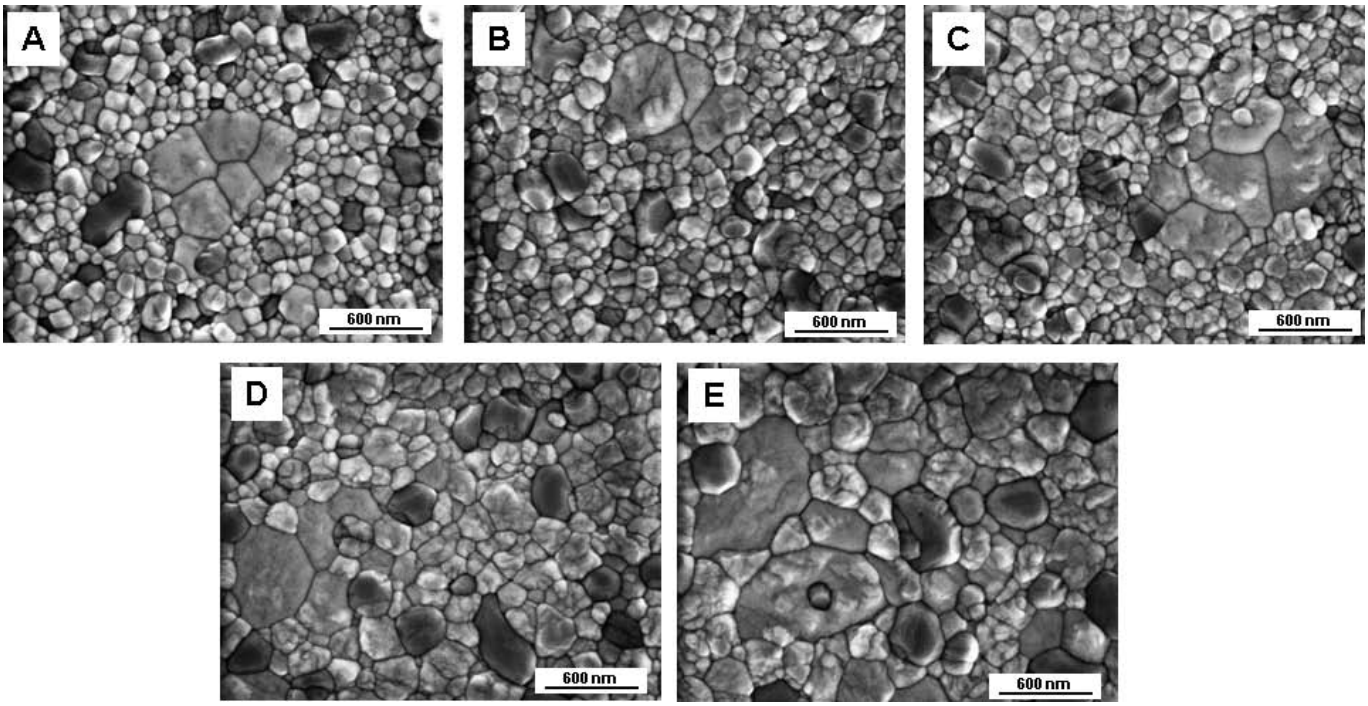

Fig. 1: SEM images of polished and thermally etched microstructure of ATZ sintered at: 1250 °C (A), 1300 °C (B), 1350 °C (C), 1400 °C(D) and 1450 °C (E).

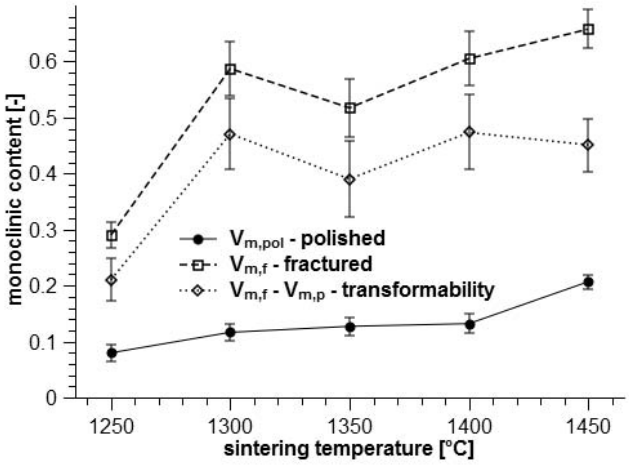

Fig. 2: Monoclinic content in polished surfaces and fracture faces and resulting transformability of ATZ vs. sintering temperature.

III. Results

(1) Microstructure

Figs. 1a-e show the microstructure of ATZ sintered at 1250 – 1450 °C. Evidently the microstructure consists of three phases. Alumina (dark grey) is homogeneously distributed in the zirconia matrix. Initially at 1250 °C the grain size of the alumina in the sintered material – 300 nm – is identical with the grain size in the powder. Coarsening of the alumina dispersion is visible between 1400 and 1450 °C, at the final temperature the grain size of alumina has grown to 500 nm. The zirconia in bright grey consists of two types of grains. At 1250 – 1350 °C small grains with a size of 100 – 200 nm and large grains of 400 – 600 nm are visible. The large grains are arranged in clusters of a few grains. Grain growth in zirconia occurs at sintering temperatures exceeding 1350 °C and proceeds further to the highest sintering temperature. Large grains grow to 800 nm and small matrix grains grow to 300 – 400 nm. The thermal etching process reveals the formation of precipitates of 150 nm in size in the larger grains that are inclined to the plane. Moreover at 1450 °C, with larger magnification, cracks in the large grains become visible at the boundaries of large grains and surrounding matrix or alumina. At some alumina/zirconia boundaries a thin layer of another phase can be identified. In order to quantify the stabilizer concentration, an EDX analysis was performed (not shown). EDX reveals that the neodymia content in the large grains is approximately 3 – 5 times higher than in the small grains. A similar ratio was found for ytterbia, however, owing to strong cross sensitivity of ytterbia with alumina, no quantitative data were obtained.

(2) Phase composition

Fig. 2 shows the monoclinic fractions of zirconia in polished surfaces and fracture faces. The difference between the two values is the transformability V_f. Monoclinic phase is present in all materials, the monoclinic content in as-fired samples rises moderately from 7 % at 1250 °C to 14 % at 1400 °C, at the final sintering temperature a more drastic increase to 20 % can be measured. Concerning the fracture faces, the monoclinic content rises from 30 % at 1250 °C to 60 % at 1300 °C, at 1350 °C the monoclinic content declines to 52 % and rises linearly to the highest monoclinic content of 68 % at a sintering temperature of 1450 °C. The resulting transformability shows an initial rise from 1250 °C to 1300 °C, then a relatively constant level of 40 – 47 % between 1300 °C and 1450 °C. Owing to error propagation, the intermediate drop at 1350 °C to ~ 40 % should not be overstressed.

Fig. 3 shows the XRD traces between 27 – 33° 2θ-scale of polished surfaces of materials sintered at 1250, 1350 and 1450 °C respectively. The shoulder in the tetragonal (101) reflex develops into a separate reflex, this reflex is the (111) reflex of cubic zirconia. Evidently the cubic content increases with sintering temperature. The corresponding XRD traces at 27 – 33° 2θ-scale of fracture faces (Fig. 4) support this presumption, while the tetragonal phase is consumed by martensitic transformation, the cubic reflex stays unchanged. In fracture faces of material sintered at 1450 °C the tetragonal phase is almost completely eliminated. It was previously suspected that additional toughening could be caused by ferroelastic domain switching of the tetragonal phase [30, 39]. The prerequisite of high tensile stress in zirconia (> 1.6 GPa) is fulfilled as residual cooling stress by CTE mismatch of alumina and zirconia added to operating stress [40]. It was therefore checked in the sample sintered at 1250 °C, which has the lowest transformability, if domain orientation has occurred by integrating the (002) and (200) reflexes of tetragonal zirconia (Fig. 5). In fact a reorientation of the tetragonal domains has occurred. The intensity ratio between I_{002}/I_{200} reflexes shifts from 0.67 in the polished surface to 0.75 in the fracture face.. According to Virkar, this indicates a domain reorientation with the (001) axes parallel to the fracture face [40]. Considering the total toughness level, the effect may only be of some importance at low sintering temperature.

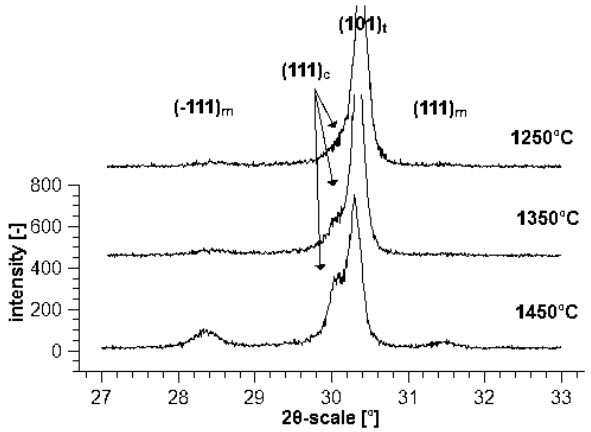

Fig. 3: XRD traces of polished surfaces of ATZ sintered at 1250, 1350 and 1450 °C in the 27 – 33° 2θ-range showing monoclinic, tetragonal and cubic reflexes.

(3) Mechanical properties

Fig. 6 shows the density and the indentation modulus of the ATZ versus sintering temperature. Both curves show a rising trend. The density shows an initial rise between 1250 and 1300 °C with subsequent flattening. It is not possible to correlate the density value to porosity alone as the phase composition is changing continuously and because the density of 1Y-2Nd-TZP is not known, SEM images of samples sintered at 1250 °C show very few small pores of ~ 100 nm in diameter which explain only half the change in density. It seems thus probable that the differing density of the sample sintered at 1250 °C is to some extent caused by incomplete stabilizer distribution. The indentation modulus E_{IND} rises almost linearly from 267 to 278 GPa. The initial rise between 1250 °C and 1300 °C may be caused by a low amount of residual porosity. A value of ~ 265 GPa can be expected based on the rule of mixture. The values of E_{IND} should not be overstressed, the indentation procedure may be susceptible to reacting to residual stress present in the samples. Moreover the microindentation process itself may create residual stress during the measurement.

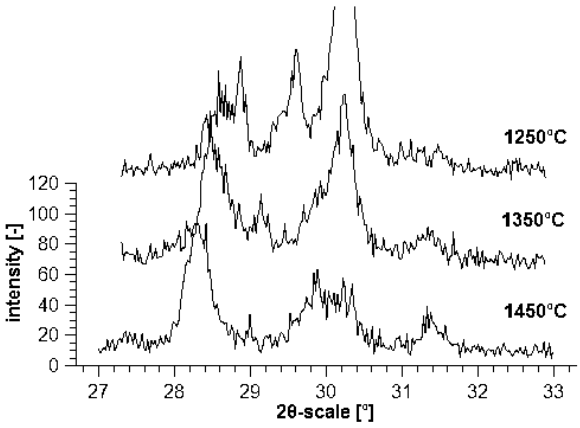

Fig. 4: XRD traces of fracture faces of ATZ sintered at 1250, 1350 and 1450 °C in the 27 – 33° 2θ-range showing monoclinic, tetragonal, cubic and additional unknown reflexes.

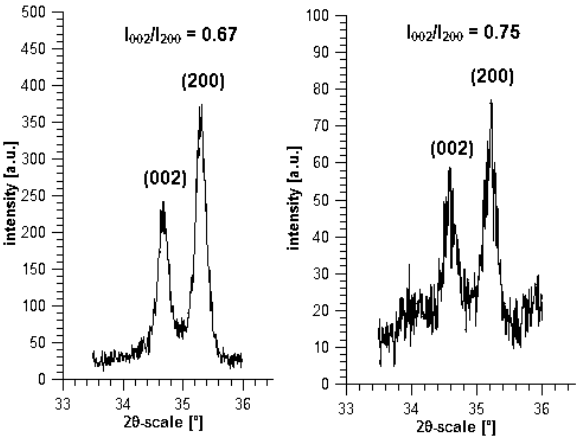

Fig. 5: XRD traces of polished surface (left) and fracture face (right) of ATZ sintered at 1250 °C in the 33.5 – 36° 2θ-range showing tetragonal (002) and (200) reflexes and their size ratio.

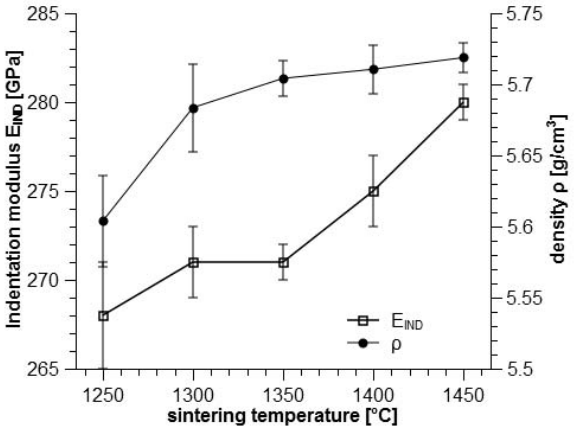

Fig. 6: Indentation modulus E_{IND} and density ϱ of ATZ vs. sintering temperature.

Fig. 7 shows the Vickers hardness HV10 and the 4-pt bending strength. The Vickers hardness shows an initial increase from 13.8 GPa at 1250 °C to 14 GPa at 1300 °C (presumably caused by residual porosity differences in stabilizer distribution) followed by a continuous decrease from this level to 13.4 GPa at 1450 °C. Compared to 2.5Y-TZP-20 vol% alumina, the hardness is slightly lower [39]. With values of 1050 – 1250 MPa for the 4-pt bending strength the ATZ reaches a very attractive level for structural ceramics. The strength rises continuously to reach its highest value at 1400 °C. At the final temperature the strength decreases, the standard deviation, however, becomes considerably smaller. Moreover, a non-linearity in the stress-strain curve in the final stage indicates a decline in Young's modulus caused by microcracking. This tendency to non-linear stress-strain curves becomes increasingly important in materials sintered at high temperatures. Fig. 8 shows-stress strain curves of the samples with the highest strength of each series for sintering temperatures of 1300 – 1450 °C. While curves are almost perfectly linear up to 1350 °C, the sample sintered at 1400 °C shows an onset of non-linearity at ~ 1000 – 1100 MPa, the material sintered at 1450 °C shows strong non-linearity starting from a stress of ~ 800 MPa (the initial kink at 400 MPa in all curves is a machine-specific artefact). According to Swain, this difference can be interpreted in terms of transformation stress σ_c or for bending test the corresponding stress σ_0 which can be analytically calculated (Eqs. 1 and 2) [4]:

$$\sigma_c = \frac{\beta \cdot (1 - \nu) \cdot K}{3\sqrt{h}} \quad (1)$$

$$\sigma_0 = \frac{3 \cdot \sigma_c}{(1 + \nu)} \quad (2)$$

K is the stress intensity coefficient, which for high toughness and R-curve domination tends to K_{tip} and for low toughness and strength controlled by defect size to K_{Ic}. Assuming a cardioid transformation zone the coefficient $\beta = 0.64$. Poisson's ratio $\nu = 0.3$, the value for h was calculated from the XRD analysis according to Kosmac [42].

For the sample sintered at 1300 °C showing high strength and intermediate toughness, flaw size control can be assumed ($K = K_{ISB} = 7.3$ MPa·√m, $h = 4$ μm), here values of $\sigma_c = 520$ MPa and $\sigma_0 = 1200$ MPa are obtained. For the very tough sample sintered at 1450 °C, R-curve domination can be expected ($K = K_{tip} = 5.2$ MPa·√m, $h = 6$ μm), here values of $\sigma_c = 317$ MPa and $\sigma_0 = 732$ MPa are obtained.

The calculated values for σ_c for the two materials are in good accord with the results of the bending tests, which show almost no deviation from linearity for the material sintered at 1300 °C and an onset of non-linearity at ~ 800 MPa for the one sintered at 1450 °C. For the materials in the transition range between these extremes, the stress intensity K for calculation of the critical transformation stress probably has a value between K_{tip} and K_{Ic}.

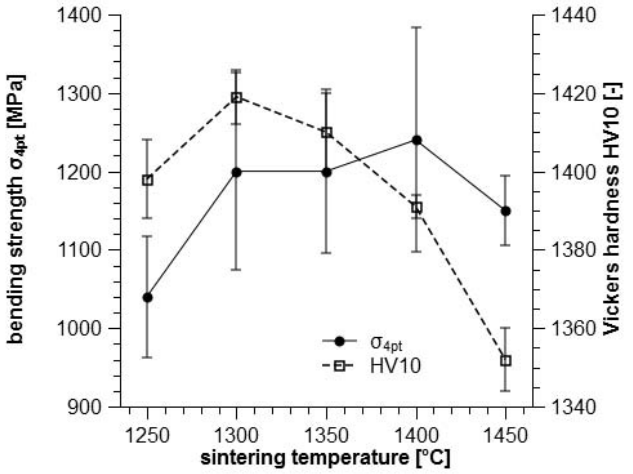

Fig. 7: Bending strength σ_{4pt} and Vickers hardness HV10 of ATZ vs. sintering temperature.

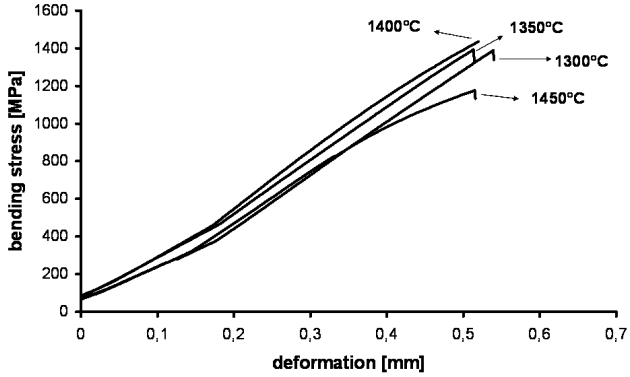

Fig. 8: Stress-strain curves of ATZ sintered at 1300 – 1450 °C determined in 4-pt bending. The curves show the samples with the highest strength of each series..

Fig. 9 shows the fracture resistance values depending on sintering temperature. The fracture resistance shows a similar trend with rising sintering temperature to that of the strength. The values for K_{ISB} rise from 6.6 MPa·√m at 1250 °C to 12 MPa·√m at 1400 °C. At 1450 °C the fracture resistance declines. The indentation fracture resistance according to Anstis shows a slightly lower level than K_{ISB}, as can be expected from a material with R-curve behaviour. It will be interesting to see whether other methods like SEVNB tests can confirm the high toughness values measured with the indentation or ISB test. The fracture resistance results of the stable indentation crack growth in bending experiments where the crack is dragged out of the initial residual stress zone are close to the K_{ISB} and K_{IND} values. In most cases, owing to the relatively short crack extension of only 20 – 35 μm, an extrapolation to K_{Ic} with the significant accuracy is very daring. For the material sintered at 1250 °C the crack extension was 150 μm, here the highest measured toughness value K_{Ic} was 6.3 MPa·√m, which is between K_{IND} and K_{ISB}, the extrapolated value of K_{Ic} was ~ 7 MPa·√m and thus more similar to K_{ISB}. In most cases, owing to the relatively short crack extension of only 20 – 35 μm and the resulting uncertainties in determining the residual stress coefficient χ (the slope of the

linear part at $K_{app} > K_{res}$), an extrapolation to K_{Ic} with the significant accuracy is very daring. The highest toughness values measured on surviving cracks can be considered a lower limit of toughness. These toughness values reach a maximum of 9 – 9.5 MPa·√m at 1400 – 1450 °C. Extrapolated values at these sintering temperatures can be as high as 15 ± 2 MPa·√m and are definitely exaggerated.

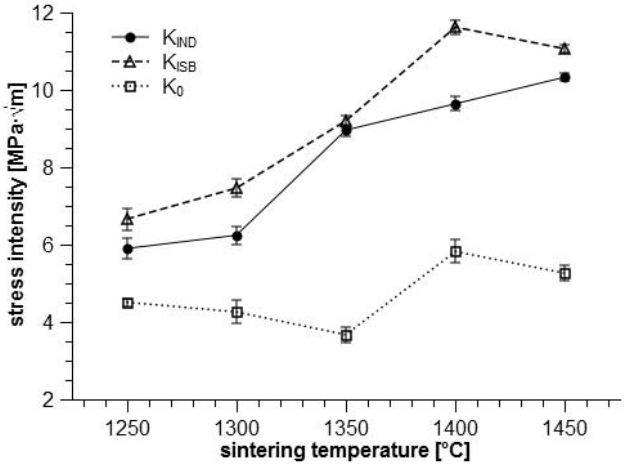

Fig. 9: Fracture resistance values K_{IND}, K_{ISB} and threshold stress intensity K_0 of ATZ vs. sintering temperature.

Threshold stress intensity K_0 shows values of around 4 MPa·√m between 1250 and 1350 °C. The peak value of 5.5 MPa·√m for K_0 is obtained at 1400 °C. This value is higher than the total toughness of coprecipitated 3Y-TZP. According to McMeeking the parameters governing the transformation toughness increment are the transformability V_f and the height of the transformation zone h [41]. The value for h was determined from XRD data according to Kosmac [42] and from the strength and toughness data according to Budiansky [43]. As the penetration depth of X-rays in zirconia is limited to a few micrometers, the calculated value for h is slightly higher. In Fig. 10, K_{ISB} is plotted versus the product $V_f \cdot \sqrt{h}$. The tentative extrapolation to the ordinate results in a value of 5.2 MPa·√m for K_{tip} the fracture resistance before the crack tip (not to be mistaken for K_0 !). This is a high value compared with 3 – 4 MPa·√m for other zirconia materials [4].

IV. Discussion

Before starting the comprehensive discussion a brief summary of the results is given.

The 1Yb-2Nd-ATZ materials produced exhibit both high strength of σ_{4pt} = 1050 – 1240 MPa (Fig. 7) and fracture resistance K_{Ic} = 6.6 – 12 MPa·√m (Fig. 9). The threshold toughness K_0 describing resistance to subcritical crack growth has a value of 4 – 5.5 MPa·√m (Fig. 9). At a sintering temperature of 1400 °C, σ_{4pt}, K_{Ic} and K_0 reach their maximum. Non-linearity in the stress-strain curves of materials sintered at 1400 °C and 1450 °C hints at R-curve behaviour (Fig. 8). The crack tip toughness K_{tip} of the materials obtained by extrapolation has a value of 5 MPa·√m (Fig. 10).

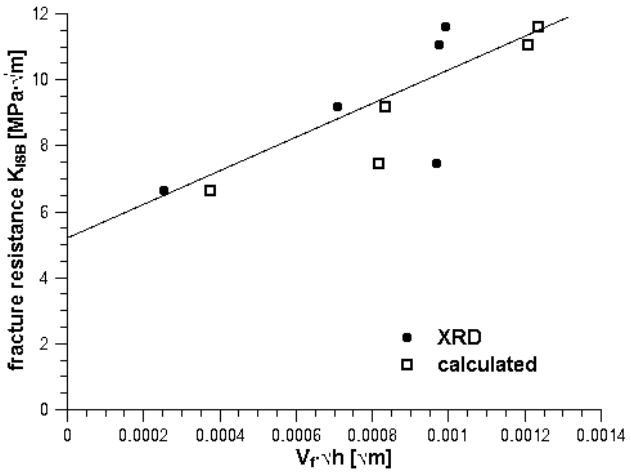

Fig. 10: Fracture resistance K_{ISB} vs. product of square root of transformation zone height h and transformability V_f measured with XRD [42] and calculated [43].

In all materials monoclinic phase is present in the as-fired state with a tendency to rise with increasing sintering temperature, the transformability of the tetragonal phase with exception of the sample sintered at 1250 °C is ~ 45 % (Fig. 2). Cubic phase appears at 1350 °C and its content increases with the sintering temperature (Fig. 3). The cubic grains are large and distributed in a fine-grained tetragonal matrix.

An explanation of the simultaneously high strength and toughness becomes possible by combining the results of mechanical characterization, phase analysis and characterization of microstructure.

Although the evolution of properties with temperature is a transient process, thermodynamic considerations are the key to understanding the behaviour of TZP or ATZ costabilized by neodymia and a smaller trivalent dopant such as ytterbia. The basics of the two binary systems can be found in phase diagrams published by Wang for Nd_2O_3-ZrO_2 and Yb_2O_3-ZrO_2 [44]. The phase boundary at 1550 K between t and t+c field in the case of Yb_2O_3-ZrO_2 is located at ~ 2 mol% Yb_2O_3, the invariant reaction T → M+F happens at 1215 K and 1.8 mol% Yb_2O_3. For the subsystem Nd_2O_3-ZrO_2 the phase boundary at 1550 K between t and t+c field in the case of Nd_2O_3-ZrO_2 is located at ~ 0.8 mol% Nd_2O_3, the invariant reaction T → M+P happens at 1326 K and 0.5 mol% Nd_2O_3. Assuming a linear correlation, we may assume that the costabilized system is supersaturated with neodymia, the initial composition is located in the t+c field which represents a miscibility gap. Thermodynamically the separation into cubic and tetragonal is favoured, but if such a separation actually takes place is a question of kinetics. The miscibility gap in coprecipitated 3Y-TZP is relatively inert at typical sintering temperatures of 1400 °C and 2 h dwell [45]. In 1Y-2Nd-ATZ a phase separation starts at a temperature as low as 1300 °C at short dwell. The initial non-homogeneous stabilizer distribution caused by the powder coating process enhances this tendency, as the stabilizer is located only at the grain surface, still initially no cubic is formed, this means that all stabilizer is first incorporated into the grains, excess stabilizer is released at higher temperature

to form cubic phase. Burger has shown that the trajectory of phase composition during sintering of coated powders is different to coprecipitated powder [46]. Stabilizers are insoluble in monoclinic, thus the incorporation of stabilizer starts once the unstabilized zirconia turns tetragonal under the influence of temperature (at ~ 1150 °C). Stabilizers then diffuse from the surface into the bulk of the grains. As the energetic situation at the surface and in the bulk is different, a certain supersaturation can be accommodated in grains having a high surface to bulk volume ratio, this makes the material sintered at low temperature very stable and less prone to transformation. Ross has shown by means of TEM that a few atomic layers of alumina, otherwise insoluble in zirconia, can be incorporated near the surface [16]. At higher sintering temperatures grains start to grow, the bulk volume increases at the expense of the surface-near volume. During fusion of smaller grains to larger grains, the stabilizer-rich region at the contact area is dragged into the grains or diffuses aside during fusion and becomes instable. The superfluous stabilizer cannot be accommodated and starts to form cubic phase. In cubic grains the stabilizer distribution is homogeneous, there is no gradient from boundary to centre (solute drag) [48]. Cubic grains thus grow faster. As the cubic takes up all the excess stabilizer and leaves the rest of the matrix with a composition at the T/T+F boundary the fine grain matrix is very transformable. Moreover at high temperature as the T+F field is wedge-shaped with the T+F/F boundary having a lower slope than the T/T+F boundary more cubic is formed at higher temperature [44]. During cooling the cubic becomes stabilizer-deficient. This should favour precipitation of tetragonal within cubic grains as a result of spinodal decomposition [49]. This effect probably causes the formation of small presumably tetragonal precipitates in the large grains of material sintered at higher temperature. This effect was not observed in 1Gd-2Nd-TZP and 1Y-2Nd-TZP systems [28, 31]. It may be speculated that the lower vertical T/T+M boundary in the Yb_2O_3-ZrO_2 system (1215 °C) compared to the Gd_2O_3-ZrO_2 system (1309 °C) can be made responsible for this behaviour. Moreover the curvature of the T/T+F boundary is different in Y_2O_3-ZrO_2 (straight) and Yb_2O_3-ZrO_2 (belly-shaped) [44, 49]. The reprecipitation of tetragonal may also cause the higher stability of the compositions sintered at high temperature compared to systems costabilized with gadolinia and yttria. The phase separation process strongly affects mechanical properties. Stabilizer depletion of the matrix grains leads to high transformability and results in high fracture resistance as a result of transformation toughening.

We may argue that considering the identical processing of all samples (except the different sintering temperature) the original flaw size in all as-fired samples is identical.

In the sample sintered at 1450 °C some microcracks are visible so that here even the existing flaw size might be larger.

As the strength does not substantially increase with toughness, the flaw sizes at the moment of fracture must be different. Flaw sizes in the tougher materials are larger but the tougher materials can tolerate larger flaws. The coarser microstructures may be more susceptible to subcritical crack growth than the finer structures. The non-linear stress-strain curves in the materials sintered at high temperature (especially at 1450 °C) are a clear indication of R-curve behaviour. In ATZ sintered at 1450 °C the zirconia is probably even more coarse, destabilized and thus transformable than at 1400 °C and reaches its critical transformation stress at 800 MPa. Once the critical transformation stress is reached, the transformation will take place without further contribution to strength (steady state). Progressive transformation of zirconia will further increase residual stress and introduce transformation-derived microcracks. This results in a reduction of Young's modulus. Large microcrack networks present critical flaws which restrict the bending strength. Especially in ATZ sintered at 1450 °C the real strength is probably somewhat lower than the measured strength owing to a shift of the neutral fibre in the bending bar to the compressive side.

According to Swain the transition from flaw size control to R-curve control in Y-TZP happens at a toughness of ~ 7 – 8 MPa·√m. In the present case K_{tip} (~ 5 MPa·√m) is higher than in Y-TZP (~ 3.5 MPa·√m). This means the intrinsic toughness is higher than in 3Y-TZP (presumably owing to a contribution by residual stress). Let us further assume the transformation mechanism is similar for all oversize trivalent dopants. We should not compare with Mg-PSZ or Ce-TZP owing to different crystallographic boundary conditions for transformation [1]. If, according to Evans, the toughness is the sum of crack tip toughness and R-curve dependent increments $K_{Ic} = K_{tip} + \Sigma\Delta K_C$, we can expect that the increase in the non-R-curve-dependent toughness will lead to higher strength at a given maximum toughness (see Eqs. 1 & 2) [50, 4].

For a deeper understanding of the phenomena and in order to confirm the data measured, other methods for measurement of toughness should be performed. Crack tip toughness may be directly measured based on crack opening displacement COD using Vickers indents or cube corner indents [51, 52]. An exact assessment of fracture toughness and a minimizing of the influence of R-curve effects on K_{Ic} can be conducted with SEVNB, in zirconia materials, however, the notch preparation has to be performed with utmost care in order to obtain reliable measurements [53, 54].

V. Conclusions

Producing alumina-toughened zirconia ceramics from ytterbia-neodymia costabilized material offers an opportunity to obtain materials with high strength, toughness and resistance to subcritical crack growth. Such ceramics may prove advantageous in the field of bioceramics and high-performance mechanical components.

The reasons identified for the favourable mechanical properties were identified in the inherent thermodynamic instability of the compositions, leading to a separation of a stabilizer-rich cubic phase. This phase separation leaves the remaining tetragonal zirconia extremely transformable. Transformation toughening is the dominant reinforcement mechanism in the composite. In materials sintered at low temperature there are some indications

that a further contribution by ferroelastic domain switching exists. The pre-existing microcracks detected in the vicinity of large grains in the material sintered at high temperature hint at a contribution of microcracking in these samples. Non-linearity in the stress-strain curve provides evidence that ATZ sintered at T ≥ 1400 °C is R-curve dominated.

References

1 Kelly, P.M., Rose, L.R.F.: The martensitic transformation in ceramics – its role in transformation toughening, *Prog. Mater. Sci.*, **47**, 463 – 557, (2002).

2 Hannink, R.H.J., Kelly, P.M., Muddle, B.C.: Transformation toughening in zirconia-containing ceramics, *J. Am. Ceram. Soc.*, **83**, [3], 461 – 87, (2000).

3 Chevalier, J., Gremillard, L., Virkar, A.V., Clarke, D.R.: The tetragonal-monoclinic transformation in zirconia: lessons learned and future trends, *J. Am. Ceram. Soc.*, **92**. [9], 1901 – 20, (2009).

4 Swain, M.V., Rose, L.R.F.: Strength limitations of transformation-toughened zirconia alloys, *J. Am. Ceram. Soc.*, **69**, [7], 511 – 18, (1986).

5 Li, P., Chen, I.W., Penner-Hahn, J.E.: Effect of dopants on zirconia stabilization – an X-ray absorption study: I, trivalent dopants, *J. Am. Ceram. Soc.*, **77**, [1], 118 – 28, (1994).

6 Li, P., Chen, I.W., Penner-Hahn, J.E.: Effect of dopants on zirconia stabilization – an X-ray absorption study: II, tetravalent dopants, *J. Am. Ceram. Soc.,* **77**, [5], 1281 – 88, (1994).

7 Li, P., Chen, I.W., Penner-Hahn, J.E.: Effect of dopants on zirconia stabilization – an X-ray absorption study: III, charge-compensating dopants, *J. Am. Ceram. Soc.*, **77**, [5], 1289 – 95, (1994).

8 Mizutani, Y., Hisada, K., Ukala, K., Sumi, H., Yokoyama, M., Nakamura, Y., Yamamoto, O.: From rare earth doped zirconia to 1 kW solid oxide fuel cell system, *J. Alloy. Comp.*, 408 – 412, 518 – 24, (2006).

9 Cao, X.Q., Vassen, R., Stoever, D.: Ceramic materials for thermal barrier coatings, *J. Eur. Ceram. Soc.*, **24**, [1], 1 – 10, (2004).

10 Nettleship, I., Stevens, R.: Tetragonal zirconia polycrystal (TZP) – a review, *Int. J. High. Tech. Ceram.*, **3**, [1], 1 – 32, (1987).

11 Singh, R., Gill, C., Lawson, B., Dransfield, G.P.: Sintering, microstructure and mechanical properties of commercial Y-TZPs, *J. Mat. Sci.*, **31**, 6055 – 62, (1996).

12 Ohnishi, H., Naka, H., Sekino, T., Ikuhara, Y., Niihara, K.: Mechanical properties of 2.0 – 3.5 mol-% Y_2O_3-stabilized zirconia polycrystals fabricated by the solid phase mixing and sintering method, *J. Ceram. Soc. Jap.*, **116**, [12], 1270 – 77, (2008).

13 Yuan, Z.X., Vleugels, J., Van der Biest, O.: Preparation of Y_2O_3-coated ZrO_2 powder by suspension drying, *J. Mat. Sci. Let.*, **19**, 359 – 61, (2000).

14 Piconi, C., Burger, W., Richter, H.G., Cittadini, A., Maccauro, G., Covacci, V., Bruzzese, N., Ricci, G.A., Marmo, E.: Y-TZP ceramics for artificial joint replacements, *Biomaterials*, **19**, 1489 – 94, (1998).

15 Kern, F.: Alumina-doped 2.5Y-TZP produced from yttria-coated pyrogenic nanopowder, *J. Ceram. Sci. Tech.*, **2**, [2], 89 – 96, (2011).

16 Ross, I.M., Rainforth, W.M., McComb, D.W., Scott, A.J., Brydson, R.: The role of trace additions of alumina to yttria-tetragonal zirconia polycrystals (Y-TZP), *Scr. Mat.*, **45**, 653 – 60, (2001).

17 Vleugels, J., Yuan, Z.X., Van der Biest, O.: Mechanical properties of Y_2O_3/Al_2O_3-coated Y-TZP ceramics, *J. Eur. Ceram. Soc.*, **22**, 873 – 81, (2002).

18 Tsukuma, K., Ueda, K., Shimada, M.: Strength and fracture toughness of isostatically hot-pressed composites of Al_2O_3 and Y_2O_3-partially-stabilized ZrO_2, *J. Am. Ceram. Soc.*, **68**, [1], $_C4-_C5$, (1985).

19 Tsubakino, H., Sonoda, K., Nozato, R.: Martensite transformation behaviour during isothermal ageing in partially stabilized zirconia with and without alumina addition, *J. Mat. Sci. Let.*, **12**, 196 – 8, (1993).

20 Kan, Y., Li, S., Wang, P., Zhang, G.J., Van der Biest, O., Vleugels, J.: Preparation and conductivity of $Yb_2O_3-Y_2O_3$ and $Gd_2O_3-Y_2O_3$ co-doped zirconia ceramics, *Solid State Ionics*, **179**, 1531 – 4, (2008).

21 Kan, Y., Zhang, G.J., Wang, P., Van der Biest, O., Vleugels, J.: Yb_2O_3 and Y_2O_3 co-doped zirconia ceramics, *J. Eur. Ceram. Soc.*, **26**, 3607 – 12, (2006).

22 Huang, S.G., Li, L., Van der Biest, O., Vleugels, J.: Microwave sintering of CeO_2 and Y_2O_3 co-stabilised ZrO_2 from stabiliser-coated nanopowders, *J. Eur. Ceram. Soc.*, **27**, 689 – 93, (2007).

23 Vleugels, J., Xu, T., Huang, S., Kan, Y., Wang, P., Li, L., Van der Biest, O.: Characterization of (Nd,Y)-TZP ceramics prepared by a colloidal suspension coating technique, *J. Eur. Ceram. Soc.*, **27**, 1339 – 43, (2007).

24 Salehi, S., Van der Biest, O., Vleugels, J.: Y_2O_3 and Nd_2O_3 co-stabilized ZrO_2-WC composites, *J. Mat. Sci.*, **43**, 5784 – 9, (2008).

25 Salehi, S., Yüksel, B., Vanmeensel, K., Van der Biest, O., Vleugels, J.: $Y_2O_3-Nd_2O_3$ double stabilized ZrO_2–TiCN nanocomposites, *Mat. Chem. Phys.*, **113**, 596 – 601, (2009).

26 Salehi, S., Vanmeensel, K., Swarnakar, A.K., Van der Biest, O., Vleugels, J.: Hydrothermal stability of mixed stabilised tetragonal (Y, Nd)-ZrO_2 ceramics, *J. Alloys. Comp.*, **495**, 556 – 60, (2010).

27 Gadow, R., Kern, F.: Novel zirconia-alumina nanocomposites combining high strength and toughness, *Adv. Eng. Mat.*, **12**, [12], 1220 – 3, (2010).

28 Kern, F.: High toughness and strength in yttria-neodymia costabilized zirconia ceramics, *Scr. Mat.*, (2012); http://dx.doi.org/10.1016/j.scriptamat.2012.05.009.

29 Kern, F., Gadow, R.: Ytterbia (2.25 mol.%) stabilised zirconia (Yb-TZP) manufactured from coated nanopowder, *Adv. Appl. Ceram.*, (2012); http://dx.doi.org/10.1179/1743676111Y.0000000071.

30 Kern, F.: 2.75Yb-TZP ceramics with high strength and aging resistance, *J. Ceram. Sci. Tech.*, **2**, [3], 147 – 54, (2011).

31 Kern, F.: Gadolinia-Neodymia-costabilized zirconia materials with high toughness and strength, *J. Ceram. Sci. Tech*., (2012) submitted.

32 Toraya, H., Yoshimura, M., Somiya, S.: Calibration curve for quantitative analysis of the monoclinic-tetragonal ZrO2 system by X-ray diffraction, *J. Am. Ceram. Soc.*, **67**, [6], C119 – 121, (1984).

33 Anstis, G.R., Chantikul, P., Lawn, B.R., Marshall, D.B.: A critical evaluation of indentation techniques for measuring fracture toughness: I, direct crack measurements, *J. Am. Ceram. Soc.*, **64**, [9], 533 – 538, (1981).

34 Chantikul, P., Anstis, G.R., Lawn, B.R., Marshall, D.B.: A critical evaluation of indentation techniques for measuring fracture toughness: II, strength method, *J. Am. Ceram. Soc.*, **64**, [9], 539 – 543, (1981).

35 Braun, L.M., Benninson, S.J., Lawn, B.R.: Objective evaluation of short-crack toughness curves using indentation Flaws: case study on alumina-based ceramics, *J. Am. Ceram. Soc.*, **75**, [11], 3049 – 57, (1992).

36 Dransmann, G., Steinbrech, R., Pajares, A., Guiberteau, F., Dominguez-Rodriguez, A., Heuer, A.: Indentation studies on Y_2O_3,-stabilized ZrO_2: II, toughness determination from sta-

ble growth of indentation-induced cracks, *J. Am. Ceram. Soc.*, **77**, [5], 1194 – 201, (1994).

37 Benzaid, R., Chevalier, J., Saadaoui, M., Fantozzi, G., Nawa, M., Diaz, L.A., Torrecillas, R.: Fracture toughness, strength and slow crack growth in a ceria-stabilized zirconia-alumina nanocomposite for medical applications, *Biomaterials*, **29**, 3636 – 3641, (2008).

38 Lube, T., Fett, T: A threshold stress intensity factor at the onset of stable crack extension of knoop indentation cracks, *Eng. Fract. Mech.*, **71**, 2263 – 2269, (2004).

39 Kern, F., Gadow, R.: Alumina-toughened zirconia from yttria-coated powders, *J. Eur. Ceram. Soc.*, (2012); http://dx.doi.org/10.1016/j.jeurceramsoc.2012.03.014

40 Virkar, A.V., Matsumoto, R.L.K.: Ferroelastic domain switching as a toughening mechanism in tetragonal zirconia, *J. Am. Ceram. Soc.*, **69**, [10], C224 – C226, (1986).

41 McMeeking, R.M., Evans, A.G.: Mechanics of transformation-toughening in brittle materials, *J. Am. Ceram. Soc.*, **65**, [5], 242 – 6, (1982).

42 Kosmac, T., Wagner, R., Claussen, N: X-ray determination of transformation depths in ceramics containing tetragonal ZrO_2, *J. Am. Ceram. Soc.*, **64**, [4], C72 – 73, (1981).

43 Budiansky, B., Hutchinson, J.W., Lambropolous, J.C.: Continuum theory of dilatant transformation toughening in ceramics, *Int. J. Solids Struct.*, **19**, [4], 337 – 55, (1983).

44 Wang, C., Zinkevich, M., Aldinger, F: Phase diagrams and thermodynamics of rare-earth-doped zirconia ceramics, *Pure Appl. Chem.*, **79**, [10], 1731 – 1753, (2007).

45 Matsui, K., Yoshida, H., Ikuhara, Y.: Isothermal sintering effects on phase separation and grain growth in yttria-stabilized tetragonal zirconia polycrystal, *J. Am. Ceram. Soc.*, **92**, [2], 467 – 75, (2009).

46 Burger, W., Richter, H.G., Piconi, C., Vatteroni, R., Cittadini, A., Boccalari, M.: New Y-TZP powders for medical grade zirconia, *J. Mat. Sci.-Mater. M.*, **8**, 113 – 118, (1997).

47 Matsui, K., Horikoshi, H., Ohmichi, N., Ohgai, M., Yoshida, H., Ikuhara, Y: Cubic-formation and grain-growth mechanisms in tetragonal zirconia polycrystal, *J. Am. Ceram. Soc.*, **86**, [8], 1401 – 1408, (2003).

48 Suto, H., Sakuma, T., Yoshikawa, N.: Discussion on the phase diagram of Y_2O_3-partially stabilized zirconia and interpretation of the structures, *Transact. Jap. Inst. Metals*, **28**, [8], 623 – 30, (1987).

49 Chen, M., Hallstedt, B., Gauckler, L.J.: Thermodynamic modeling of the $ZrO_2 – YO_{1.5}$ system, *Solid State Ionics*, **170**, 255 – 274, (2004).

50 Evans, A.G: Perspective on the development of high toughness ceramics, *J. Am. Ceram. Soc.*, **73**, [2], 187 – 206, (1990).

51 Fünfschilling, S., Fett, T., Oberacker, R., Hoffmann, M.J., Schneider, G.A., Becher, P.F., Kruzic, J.J.: Crack-tip toughness from vickers crack-tip opening displacements for materials with strongly rising R-curves, *J. Am. Ceram. Soc.*, **94**, [6], 1884 – 1892, (2011).

52 Cuadrado, N., Casellas, D., Anglada, M., Marro, F.G.: Fracture toughness evaluation by crack-opening displacement of cube-corner indenters, In: Proceedings of the 13th interregional conference on ceramics CIEC13, Universitad Polytécnica de Catalunya, Barcelona, Spain, (2012).

53 Krell, A.: Features of notch preparation for fracture toughness measurements in partially stabilized zirconia, *J. Am. Ceram. Soc.*, **77**, [2], 600 – 602, (1994).

54 Wang, J., Rainforth W.M., Wadsworth, I., Stevens, R: The effects of notch width on the SENB toughness for oxide ceramics, *J. Eur. Ceram. Soc.*, **10**, [1], 21 – 31, (1992).